X-RAY PHOTOELECTRON RAMAN ULTRAFAST SPECTROSCOPY OF HIGH ENTROPY NANOPARTICLES

S.Srividhya

Dept of Physics, Indian Maritime University, Chennai campus

Dr.P.Sangeetha

Dept of Physics, Arignar anna government arts college, Cheyyar

Abstract

The synthesis of high entropy (HE) nanoparticles (NPs) is a challenging procedure in terms of scalability, cost and process complexity, high entropy nanoparticle shape modification, and synthesis speed. Arrangement state was confirmed by energy-dispersive X-ray ultrafast spectroscopy investigation with aberration correction used analyse synthesised.The main characteristics of are revealed by results Raman ultrafast spectroscopy analysis, selected area electron diffraction, and X-ray diffraction, which are in line with the Scanning transmission electron microscopy (STEM) findings.

1. Introduction

This requirement will be met, which our group initially used to investigate the charge transfer pathway of photogenerated electrons [1]. Using ISI-XPS, it is possible to determine if a particular catalyst component acquires or loses electrons by comparing the binding energies of matching components during the testing procedure with and without light stimulation [2].

Therefore, it is challenging but desirable to design a system that integrates the extra physics gain effect with in situ characterization techniques in order to convert the "black box" battery into a "see-through" battery that permits direct observation of the electro catalytic reaction sites and routes.Unfortunately, the increase in elevate any further [3]. Most people agree that the latter problem is caused by faults [4].

Moreover, stannite structure—which is more common for CZTS—seems to be more beneficial for AZTS than kesterite structure. For flexible photovoltaic (PV), in example, one way to create a thin absorber layer is to produce nanoparticles (NPs) in a colloidal solution. Next, an NP layer is applied a (flexible) substrate [1,12].

Flexible PV devices provide benefits over PV cells on glass for future applications because of affordable roll-to-roll techniques [13]. It has been demonstrated that Raman spectroscopy is a widely used method for structural characterisation of CZTS and several related substances its remarkable, sample pre-treatment is not required for Raman spectroscopy.

Moreover, it has the ability to directly probe NPs in the solutions as synthesised. Because of these benefits, Raman spectroscopy makes it possible to thoroughly screen the synthesis conditions of novel NP compounds, especially by carefully varying each component over the whole compositional range.Because of this, we decided to use Raman spectroscopy as the main way of characterising the CAZTS and AZTS NCs in this study.

We achieved this by applying a technique that we have discovered to be efficient in generating high. But small number of articles on colloidal high entropy nanoparticles was undertaken on the latter [15].

2. Materials

It has the capacity to directly probe the synthesised high entropy NPs in the solutions.

These advantages allow Raman ultrafast spectroscopy to be used to completely screen the synthesis conditions of new high entropy NP compounds, especially when each component is carefully varied throughout the whole compositional range.

Table 1.FWHM, regions, and multiplet peak locations were utilised to match the XPS data.

Name		Binding energy	FWHM	Area (%)
Maghemite	Maghemite	733.17	1.2	2.2
mixture	Maghemite	697.21	1.1	8.0
	Maghemite	702.14	1.4	17.1
	Maghemite	698.45	1.6	23.4
	Maghemite	703.87	1.5	21.9
	Fe(III) magnetite	721.97	3.2	1.9
	Fe(III) magnetite	714.17	2.5	1.7
	Fe(III) magnetite	699.21	2.1	3.8
	Fe(III) magnetite	734.42	2.7	4.1
	Fe(III) magnetite	699.32	2.0	0
	Fe(III) magnetite	718.48	2.1	4.2
	Fe(III) magnetite	726.70	2.6	3.8
Maghemite	Maghemite	758.45	2.0	3.7
	Maghemite	721.55	2.0	8.6
	Maghemite	715.42	2.2	19.7

Maghemite	755.21	2.0	26.6
Maghemite	702.35	1.6	26.9
Fe(III) magnetite	756.32	3.5	5.0
Fe(III) magnetite	721.21	1.0	1.1
Fe(III) magnetite	732.13	2.8	1.2
Fe(III) magnetite	745.25	2.1	1.9
Fe(III) magnetite	699.15	2.6	4.0
Fe(III) magnetite	678.44	2.4	1.9
Fe(III) magnetite	684.15	2.5	2.0
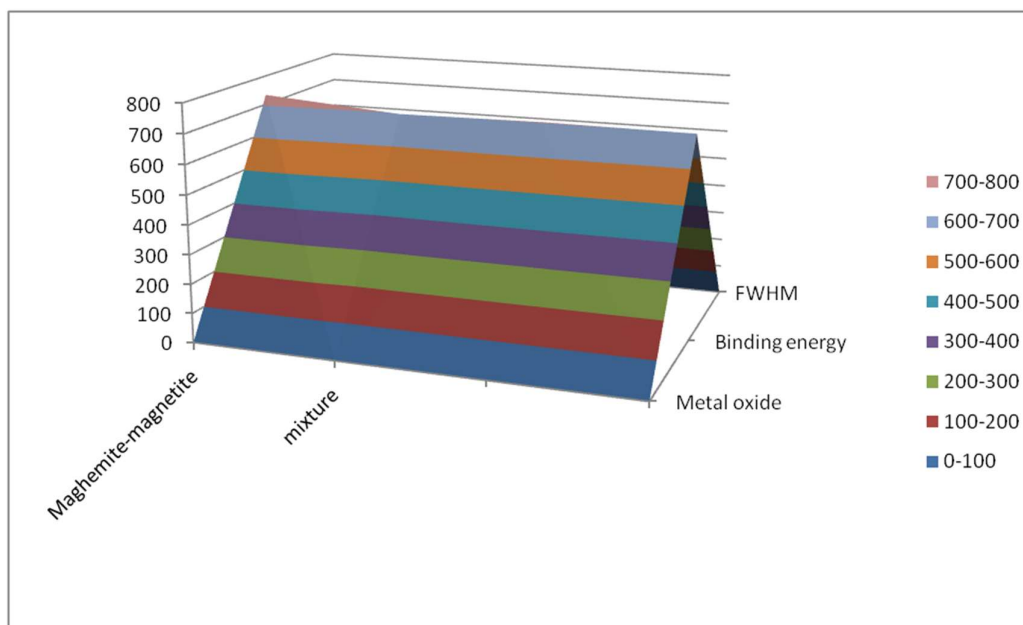
Figure 1. Regions utilised to match the ultrafast XPS data, multiplet peak locations, and FWHM.
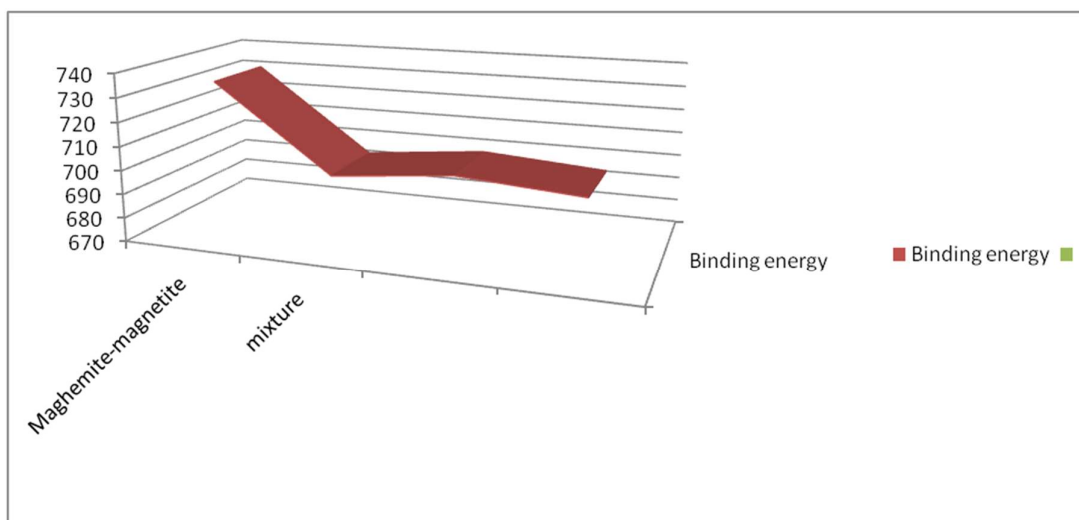
Figure 2. Binding energy of high entropy NPs.
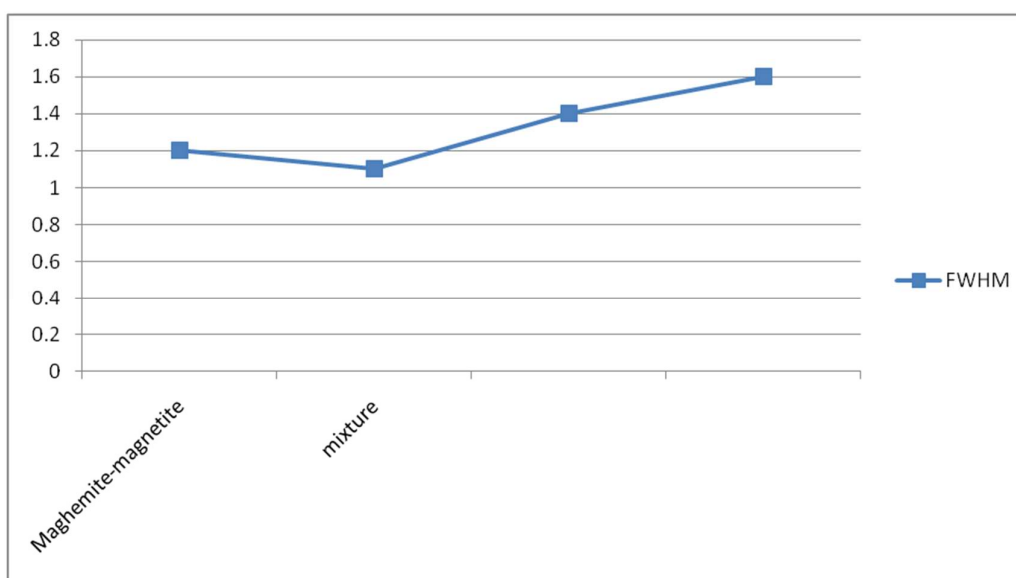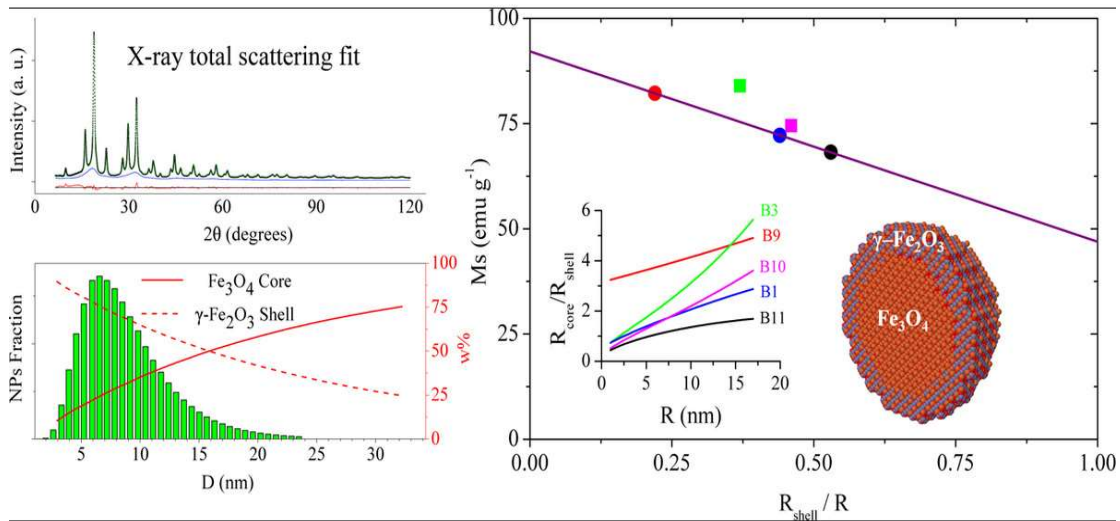

Figure 3. FWHM to match ultrafast XPS data.

Figure 4. High entropy nanoparticles in the 5-15 nm Range

3. Results and discussion

3.1. XPS and Raman spectroscopy

Every spectrum was measured using a KratosAxis Ultrafast XPS. Using the silver Fermi edge, the resolution function of the instrument was found to be 0.48 eV. Sample charge throughout each experiment. For the survey scans, the following settings were applied: pass energy = 156 eV, sweep time = 177 s, step size = 0.9 eV, and energy range = 1100–0 eV.

A high-resolution spectrum was achieved, depending on the peak that was being studied. Using an aperture of 680 m by 150 m and a penetration depth of 12 nm, the sample's ultrafast XPS sampling volume was about 100 m3.

For analysis, dry mineral samples were broken in a hoover to create new, clean faces. Both elastic (Rayleigh scattering) and inelastic (Raman scattering) dispersion of the photons occurs. Inverse length units are used to express wave numbers in Raman ultrafast spectra. The volume of the samples used in the Raman macro mode is almost 20 times more than that of the ultrafast XPS.

Fe(III) in solution would lead to the development of hydrated ferric oxides (HFO) high entropy nanoparticles since magnetite oxidises to produce maghemite, that water molecules or hydroxyl ions that share Fe's lone electron pair coordinate with iron oxide surfaces. As a result, Lewis acids, like water, react with surface Fe atoms.
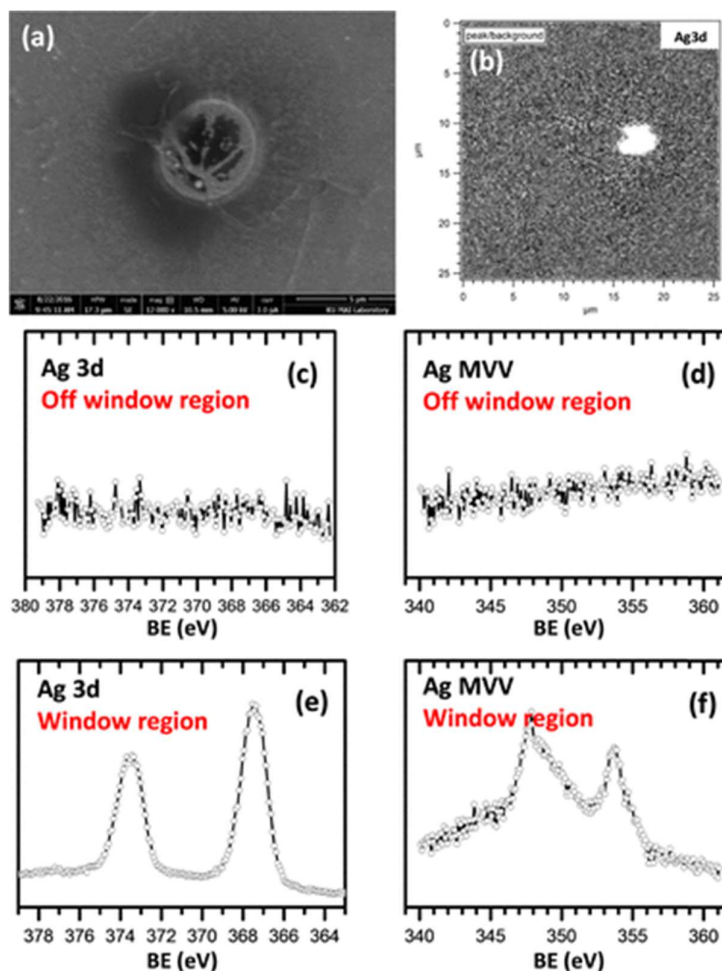
Figure 5. High entropynanoparticle X-ray photoelectron spectroscopy

Figure 5 displays the potential phases of high entropy nanoparticle production through an FSP pathway. In summary, the mechanism of gaseous phase to particle formation is examined.Microdroplets that were at room temperature in an atmospheric environment were produced as aerosol sprays using the spray nozzle.

Upon approaching the flame zone during the first stage of pyrolysis, there may be an immediate vaporisation of the solvent and evaporation of the metal precursor. Gaseous metal oxides may be produced instantaneously by reacting vaporised metal with surrounding oxygen.

Energy-dispersive X-ray ultrafast spectroscopy analysis with aberration correction was utilised to confirm the arrangement state. Results from Raman ultrafast spectroscopy analysis, selected area electron diffraction, and X-ray diffraction, which are consistent with Scanning transmission electron microscopy (STEM) findings, demonstrate the major properties of STEM.

Maghemite–magnetite high entropy nanoparticles, as opposed to microporous adsorption, have the ability to absorb metal rapidly because of external surface adsorption. Moreover, the adsorption of Cr(VI) on the mixture of magnetite and maghemite can include two different processes. First, Cr(VI) species move to the adsorbent's outer particle surface for contact (film diffusion) from the bulk fluid phase.

Conclusion

High entropy nanoparticle (NP) synthesis difficult process in terms of scalability, cost, complexity of the process, customization of high entropy nanoparticle form, and speed of synthesis. Using aberration employed synthetic.The results of selected area electron diffraction, X-ray diffraction, and Raman ultrafast spectroscopy of high entropy nanoparticles investigation all support the Scanning transmission electron microscopy (STEM) findings and highlight the primary features.

References

1. Zhang, X.; Fu, E.; Wang, Y. Fabrication of Cu2ZnSnS4 (CZTS) Nanoparticle Inks for Growth of CZTS Films for Solar Cells. Nanomaterials 2019, 9, 336.

2. Nazligul, A.S.; Wang, M. Recent Development in Earth-Abundant Kesterite Materials and Their Applications. Sustainability 2020, 12, 5138.

3. Giraldo, S.; Jehl, Z.; Placidi, M.; Izquierdo-Roca, V.; Pérez-Rodríguez, A.; Saucedo, E. Progress and Perspectives of Thin Film Kesterite Photovoltaic Technology: A Critical Review. Adv. Mater. 2019, 31, 1806692.

4. Gershon, T.; Bishop, D.; Antunez, P.; Singh, S.; Brew, K.W.; Lee, Y.S.; Gunawan, O.; Gokmen, T.; Todorov, T.; Haight, R. Unconventional Kesterites: The Quest to Reduce Band Tailing in CZTSSe. Curr. Opin. Green Sustain. Chem. 2017, 4, 29–36.

5. Yu, X.; Cheng, S.; Yan, Q.; Yu, J.; Qiu, W.; Zhou, Z.; Zheng, Q.; Wu, S. Efficient (Cu1−xAgx) ZnSn (S,Se) Solar Cells on Flexible Mo Foils. RSC Adv. 2018, 8, 27686–27694.

6. Wu, Y.; Sui, Y.; He, W.; Zeng, F.; Wang, Z.; Wang, F.; Yao, B.; Yang, L. Substitution of Ag for Cu in Cu2ZnSn (S,Se) : Toward Wide Band Gap Absorbers with Low Antisite Defects for Thin Film Solar Cells. Nanomaterials 2020, 10, 96.

7. Romanyuk, Y.E.; Haass, S.G.; Giraldo, S.; Placidi, M.; Tiwari, D.; Fermin, D.J.; Hao, X.; Xin, H.; Schnabel, T.; Kauk-Kuusik, M.; et al. Doping and Alloying of Kesterites. J. Phys. Energy 2019, 1, 044004.

8. Liang, X.; Wang, P.; Huang, B.; Zhang, Q.; Wang, Z.; Liu, Y.; Zheng, Z.; Qin, X.; Zhang, X.; Dai, Y. Effects of Ag Incorporation on the Band Structures and Conductivity Types of (Cu1−xAgx)2 ZnSnS4 Solid Solutions. ChemPhotoChem 2018, 2, 811–817.

9. Liu, N.; Xu, F.; Zhu, Y.; Hu, Y.; Liu, G.; Wu, L.; Wu, K.; Sun, S. Synthesis and Characterization of (Cu1−xAgx)2ZnSnS4 Nanoparticles with Phase Transition and Bandgap Tuning. J. Mater. Sci. Mater. Electron. 2020, 31, 5760–5768.

10. Tsuji, I.; Shimodaira, Y.; Kato, H.; Kobayashi, H.; Kudo, A. Novel Stannite-Type Complex Sulfide Photocatalysts AI 2 -Zn-AIV-S2 (AI = Cu and Ag; AIV = Sn and Ge) for Hydrogen Evolution under Visible-Light Irradiation. Chem. Mater. 2010, 22, 1402–1409.

11. Saha, A.; Figueroba, A.; Konstantatos, G. Ag2ZnSnS4 Nanocrystals Expand the Availability of RoHS Compliant Colloidal Quantum Dots. Chem. Mater. 2020, 32, 2148–2155.

12. Stroyuk, O.; Raevskaya, A.; Gaponik, N. Solar Light Harvesting with Multinary Metal Chalcogenide Nanocrystals. Chem. Soc. Rev. 2018, 47, 5354–5422. [CrossRef]

13. D. Blowes, Trackinghexavalent Cr in groundwater, Sci.J. 295 (2002) 2024–2025. [2] J.O. Nriagu, E. Nieboer, Historical Perspectives. Chromium in the Natural and Human Environments, 20, John Wiley & Sons, New York, 1988, pp. 1–20.

14. C.D. Palmer, P.R. Wittbrodt, Processes affecting the remediation of chromiumcontaminated sites, Environ. Health Perspect. 92 (1991) 25–40.

15. F.C. Richard, A.C.M. Bourg, Aqueous geochemistry of chromium: a review, Water Res. 25 (1991) 807–816.

16. L. Dupont, E. Guillon,Removalofhexavalentchromiumwithalignocellusic substrate extracted from wheat bran, Environ. Sci. Technol. 37 (2003) 4235–4241.

17. D.B. Singh, G.S. Gupta, G. Prasad, D.C. Rupainwar, The use of Hematite for Cr(VI) removal, J. Environ. Sci. Health A28 (8) (1993) 1813–1826.

18. Q. Pang, X. Liang, C. Y. Kwok, L. F. Nazar, Nat. Energy 2016, 1, 16132.

19. L. Peng, Z. Wei, C. Wan, J. Li, Z. Chen, D. Zhu, D. Baumann, H. Liu, C. S. Allen, X. Xu, A. I. Kirkland, I. Shakir, Z. Almutairi, S. Tolbert, B. Dunn, Y. Huang, P. Sautet, X. Duan, Nat. Catal. 2020, 3, 762.

20. C. Yang, J. Chen, X. Ji, T. P. Pollard, X. Lu, C. J. Sun, S. Hou, Q. Liu, C. Liu, T. Qing, Y. Wang, O. Borodin, Y. Ren, K. Xu, C. Wang, Nature 2019, 569, 245. [4] S. H. Chung, A. Manthiram, Adv. Mater. 2019, 31, 1901125.

21. Y. Zhang, Z. Wu, S. Wang, N. Li, S. R. P. Silva, G. Shao, KWangP. Zhang, InfoMat 2022, 4, e12294.